Characterization of DNA Origami Nanostructures for Size and Concentration by Dynamic Light Scattering and Nanoparticle Tracking Analysis

Qiaochu Zhang[1], Alireza Ebrahimimojarad[1], Akshay Shah[2], and Jinglin Fu*[1,2]

[1]Department of Chemistry, Rutgers University–Camden, Camden, NJ 08102, USA.

[2]Center for Computational and Integrative Biology, Rutgers University–Camden, Camden, NJ 08102, USA.

*Corresponding Author: Jinglin Fu, jinglin.fu@rutgers.edu

Abstract

Nucleic acids self-assembly has rapidly advanced to produce multi-dimensional nanostructures with precise sizes and shapes. DNA nanostructures hold great potential for a wide range of applications, including biocatalysis, smart materials, molecular diagnosis, and therapeutics. Here, we present a study of using dynamic light scattering (DLS) and nanoparticles tracking analysis (NTA) to analyze DNA origami nanostructures for their size distribution and particles concentrations. Compared to DLS, NTA demonstrated higher resolution of size measurement with a smaller FWHM and was well suited for characterizing multimerization of DNA nanostructures. We future used intercalation dye to enhance the fluorescence signals of DNA origami to increase the detection sensitivity. By optimizing intercalation dyes and the dye-to-DNA origami ratio, fluorescent NTA was able to accurately quantify the concentration of dye-intercalated DNA nanostructures, closely matching with values obtained by UV absorbance at 260 nm. This optimized fluorescent NTA method offers an alternative approach for determining the concentration of DNA nanostructures based on their size distribution, in addition to commonly used UV absorbance quantification. This detailed information of size and concentration is not only crucial for production and quality control but could also provide mechanistic insights in various applications of DNA nanomaterials.

Keywords: DNA origami, nucleic acids self-assembly, dynamic light scattering, nanoparticle tracking analysis, size distribution and concentration

1. INTRODUCTION

In recent decades, the rapid advancement of nucleic acids self-assembly has enabled the precise design and creation of multi-dimensional nanostructures with controlled sizes and shapes.[1] Due to their programmable and addressable assembly, DNA nanostructures are often used as frameworks to direct the assembly of other elements at the nanoscale[2] and organize their spatial arrangement.[3, 4] Such examples include the assembly of multienzymes on DNA nanostructures, [5-7] spatial arrangement of ligands,[3, 8] and engineering of biomimetic nanostructures,[9, 10] as well as spatially-regulated plasmonic nanomaterials[11, 12] Functionalized DNA nanostructures hold great potential for various applications such as molecular diagnosis,[13] drug and gene delivery,[14-16] vaccine development[17] and energy-transfer materials.[18-20] Accurate characterization of the shape and size distribution of DNA nanostructures is not only crucial for production and quality control, but is also important for gaining mechanistic insights in various applications of DNA nanomaterials.

Atomic force microscopy (AFM) and transmission electron microscopy (TEM) are commonly used to visualize the structural details of 2D and 3D DNA nanostructures. Although AFM and TEM can perform super-resolution imaging of DNA nanostructures on a surface that absorbs nanoparticles or under cryo conditions at low temperature, these methods may not provide an accurate representation of the actual sizes and properties of DNA nanostructures in solution. Several experimental and simulations have suggested that DNA nanostructures are soft and flexible in solution, likely resulting in wrapped and twisted structures.[21-23] Therefore, it remains necessary to acquire size and shape data for soluble DNA nanostructures, which will assist in interpreting the size distribution of nanoparticles, as well as the presence of aggregation or degradation in solution. Another potential issue is that the concentration of DNA nanostructures

is generally determined by UV absorbance of nucleic acids at 260 nm. However, UV absorbance quantified the total concentration of dsDNA, without considering the structural integrity and the purity of DNA nanostructures. Developing an alternative method to assess the concentration of DNA nanoparticles based on their size distribution, in addition to UV absorbance, would be beneficial to the field.

Dynamic Light Scattering (DLS), also known as Quasi-Elastic Light Scattering, is a non-invasive, well-established technique for measuring the size distribution of molecules and nanoparticles typically in the submicron range, when dispersed in solution.[24, 25] Brownian motion describes the random movement of particles that is induced by the bombardment of the solvent molecules. Larger particles exhibit slower Brownian motion compared to smaller particles. As shown in **Figure 1A**, the Brownian motion of particles causes laser light to be scattered at different intensities, fluctuations, and angles. Analyzing these fluctuations in scattering intensity allows for the estimation of the velocity of Brownian motion. The correlation decay $G(\tau)$ of the scattered light intensity gives the diffusion coefficient (D_{diff}) of a particle by: [24, 26]

$$G(\tau) = A[1 + B\, exp(-2\Gamma t)] \qquad (1)$$

where A is the baseline of the correlation function, B is the intercept of the correlation function. Γ is determined by:

$$\Gamma = D_{diff} * q^2 ; \quad q = \left(\frac{4\pi n}{\lambda_0}\right) * \sin\left(\frac{\theta}{2}\right) \qquad (2)$$

where q is determined by refractive index (n) of the solvent, wavelength of the laser (λ_0), and the scattering angle (θ).[27] The hydrodynamic radius (R_H) of particles can be estimated by the Stokes-Einstein equation:

$$R_H = \frac{k_B T}{3\pi\eta D_{diff}} \quad (3);$$

where k_B is Boltzmann's constant, η is the solvent viscosity.

DLS is capable of measuring particle sizes ranging from 1 nm to a few μm based on factors such as relative number, particle volume and scattering intensity. Modern DLS systems are adapted to measuring sizes of biomacromolecules in solution, including proteins, nucleic acids nanostructures, and lipid vesicles. DLS may also be used to estimate the molecular weight of macromolecules and vesicles.[28] However, DLS lacks the resolution needed to analyze multiple components and multimerization of nanoparticles.[15] Moreover, soft nanoparticles composed of biopolymers exhibit weaker scattering signals than solid and metallic particles,[16] making DLS less sensitive for analyzing biomolecular nanoparticles.

Nanoparticle tracking analysis (NTA) is a recently developed technique that enables the direct tracking and analysis of individual nanoparticles diffusion.[29, 30] In **Figure 1B**, a laser beam (~ 50 μm wide) illuminates a sample chamber, where suspended particles cause light scattering. The scattered light from particles is collected by a long working-distance objective that is positioned at 90° to the illumination plane.[17,19]A high-frame-rate camera (such as CMOS) operating at ~ 30 to a few hundred frames per second is used to record a video of particles moving under Brownian motion within a field of view (e.g. ~ 100 μm × 80 μm × 10 μm for Malvern Nanosight). NTA can also detect fluorescence signal emitted by fluorescent particles to track their movement. The NTA software analyzes the movement traces of individual particles and directly determines the diffusion coefficient by measuring the mean squared displacement of a particle in one, two or three dimensions. For example, the displacement in two dimensions ($\overline{(x,y)^2}$) can be used to calculate the R_H by Stokes-Einstein equation:

$$D_{diff} = \frac{\overline{(x,y)^2}}{4} = \frac{k_B T}{3\pi\eta R_H} \; ; \quad \frac{\overline{(x,y)^2}}{4} \; is \; the \; mean \; squared \; displacement \; in \; 2D \qquad (4) \; ;$$

NTA can be used to measure particles concentration by counting the number of particles detected in a specified volume. In comparison to DLS, the particle-by-particle tracking should provide high-resolution results for nanoparticles' size distribution and concentration. Additionally, NTA and DLS complement each other in size measurement. NTA is suitable for larger nanoparticles or aggregates exceeding 50 nm in diameter, while DLS can measure smaller particles as tiny as a few nanometers, such as linear peptides, nucleic acids, and protein monomers. Both DLS and NTA has proven effectiveness in characterizing various nanoscale particles[22], including solid and metallic nanoparticles[22], liposomes[23], extracellular vesicles[24], viruses[25], and protein aggregates[20].

Here, we reported a study of using DLS and NTA to analyze DNA origami nanostructures for their size distribution and concentrations. We compared the resolution, sensitivity, and reliability of measurements between DLS and NTA. Additionally, we optimized fluorescent NTA for the sensitive and robust measurement of the concentration and size for DNA nanostructures.

2. MATERIALS AND METHODS

2.1. Materials. DNA origami staples were prepared by customer-synthesized oligonucleotides from Integrated DNA Technologies. M13 single-stranded DNA was purchased from Bayou Biolabs. 50 nm gold nanoparticles (AuNP) were purchased from Sigma-Aldrich. Intercalating dye of DiYO™-1 (λ_{ex}~ 483 nm and λ_{em} ~501 nm) was purchased from AAT Bioques. QuantiFluor® dsDNA (λ_{ex}~ 501 nm and λ_{em} ~531nm) were ordered from Promega.

2.2. Preparation of Buffer Solutions. All buffers were prepared using either deionized water or distilled water. 1× TAE -12.5 mM Mg^{2+} (pH 8) buffer solution includes 40 mM Tris, 20 mM acetic acid, 2 mM EDTA, and 12.5 mM magnesium acetate, which is prepared by adding 100 mL of a 10× TAE stock solution into 900 mL of deionized water as described in previously published protocols.[31, 32]

2.3. Preparation of DNA Origami. Rectangular and triangular DNA origami structures were designed by TIAMAT and CADNANO as reported previously.[5, 33] 100 µL solution containing 20 nM single-stranded M13mp18 DNA (M13, 7249 nucleotides) and 5 fold molar excess of staple strands were thermally incubated under an annealing program with the temperature gradually transitioning from 95 to 4 °C as detailed in **Table S1**. Subsequently, excess and free staple strands were removed by centrifugation with 100 kD-cutoff Amicon filters (500 µL) in 1× TAE -12.5 mM Mg^{2+} (pH 8) buffer for three times.[31, 34] The concentration of the purified DNA origami solution was determined by the absorbance at 260 nm, with an assumed extinction coefficient of ~109119009 M^{-1} cm^{-1} for the M13-scaffolded DNA origami. The detailed staple sequences are listed in the supporting information **Table S2 and S3**.

2.4. DLS and NTA characterization of DNA nanostructures. A Zetasizer Pro (Malvern Panalytical) was used for DLS experiments as reported previously.[14, 35] All buffer solutions used for DLS experiments were filtered by a 0.2 µm syringe filter. Before measurement, a disposal cuvette was rinsed three times by distilled water. 100 µL of ~ 5 - 10 nM DNA origami solution was added into the cuvette to measure the hydrodynamic diameter (d.i.) of DNA nanoparticles by light scattering.

A Nanosight 300 (Malvern Panalytical) was used for NTA experiments. Prior to the measurement, all buffer solutions used for experiments were filtered by a 0.2 µm syringe filter.

DNA sample was diluted in buffer to a concentration of ~ 10^7-10^9 particles/mL, which was equivalent to a molar concentration of 16.67 fM - 1.67 pM.A Laser Module of 488 nm was used for NTA measurement. Prior to the measurement, a PDMS gasket was attached and sealed to the detection glass, forming a solution chamber. The Laser Module was gently pushed into a track to touch with the power connector. The "NanoSight NTA 3.4" software was used to operate the NTA measurement. The system was first flushed by a water or buffer solution until a clean background shown by the imaging camera. Then, ~ 500 µL to 1 mL sample was loaded into a 1 mL syringe which was mounted onto a pump to control the flow speed. The flow rate was set at 100 in control software for NTA to capture a video of tracking particles movement. The measurement was generally repeated for at least three times with optimized "Screen Gain" and "Camera Level". A "Detection Threshold" of 2 – 3 was used for analyzing DNA nanoparticles.

2.5. Atomic force microscope (AFM) imaging and Dynamic light scattering (DLS). DNA nanostructures were imaged in liquid by AFM using the published protocol.[14, 31, 34] 2 µL of enzyme-origami solution was first deposited onto a freshly cleaved mica surface (Ted Pella, Redding, CA) and was left to adsorb for 2 minutes. Then, 80 µL of 1 × TAE- 12.5 mM Mg^{2+} buffer was added to the Mica for scanning in liquid. 2 µL of 100 mM Ni^{2+} were also added to enhance DNA adsorption on mica. The samples were scanned by the "Scanasyst mode in liquid mode" of Multimode 8 AFM (Bruker, Billerica, MA), using "SCANASYST-Fluid + probe". For best imaging quality, the peak force setpoint was kept at ~ 100 – 150 pN.

2.6. Data Analysis and Fitting. Nanoparticle track analysis software (Marven), GraphPad Prism and Origin were used for analyzing data and plotting curves. Peak analysis utilized the Gauss Fit method in Origin.

3. RESULTS AND DISCUSSION

We first characterized a rectangular DNA origami by DLS. Because the particle scattering intensity is not linearly proportional to the size of particles, DLS generally gives the size distribution based on three modes of number (or population), volume, and signal intensity. In the supporting information **Figure S1**, the "Number" mode prioritized to show nanoparticles with a smaller mean size at ~80 nm because they took up the major population, while the "Intensity" mode preferred to show larger nanoparticles with a mean size at ~ 110 nm due to their strong scattering signals and the "Volume" mode balanced the number and scattering intensity of nanoparticles with a mean size at ~ 93 nm. In **Figure 2A**, DLS measurement of a rectangular DNA origami ("Number" mode) showed a broad peak spanning from ~ 50 to 150 nm, with the highest peak observed at ~ 81 nm. The peak fitting analysis identified two potential peaks at ~ 78 nm and 104 nm. In **Figure 2B**, the direct track of individual DNA nanoparticles by scattering NTA showed two well separated peaks at ~ 55 nm and ~ 92 nm. The major population (> 90%) at the size of ~ 55 nm represented a single rectangular DNA origami tile and the minor population (<10%) at the size of ~ 92 nm was attributed to the dimer of DNA origami tiles. In **Figure 2C**, AFM images showed a rectangular DNA origami at an average size of ~ 60 nm × 100 nm on 2D mica surface. However, in the solution, single-layer DNA origami was quite structurally flexible and could be wrapped over or twisted into smaller sizes as indicated by the simulation,[22] electron microscope [23] and X-ray scattering.[21] Next, we compared DLS and NTA for measuring a triangular DNA origami which had π- π stacking induced multimer formation.[33, 36] In **Figure 2D**, DLS characterization of triangular DNA origami exhibited a very broad peak spanning from ~ 50 to 250 nm. The presence of DNA origami multimers posed a challenge for analysis resolution in DLS. In contrast, scattering NTA revealed three distinct peaks at ~ 66 nm (monomer), 125 nm (dimer), and 196 nm (trimer) as

shown in **Figure 2E**. The formation of multimer DNA origami was also confirmed by AFM imaging (**Figure 2F**) which clearly showed monomers, dimers, and trimers of triangular DNA origami. In **Table 1**, we assessed the resolution of size measurements by the full width at half maximum (FWHM) of peaks for DLS and NTA. NTA analysis consistently exhibited smaller FWHM values for peaks (e.g. 16 nm for peak 1 in rectangular origami) compared to those obtained with DLS (e.g. 28 nm for peak 1 in rectangular origami), suggesting superior measurement resolution with NTA over DLS. The scattering NTA is also more sensitive than DLS for detecting DNA origami nanostructures. Typically, DLS can detect DNA origami samples at a minimum concentration of a few nanomolar. NTA can detect DNA origami at around 1 pM, which is at least a three-order-of-magnitude lower concentration than that required by DLS. The design shapes of rectangular and triangular origamis were shown in the supporting information **Figure S2 and S3**.

While scattering NTA demonstrated greater sensitivity and higher resolution than DLS, the relatively weak scattering signals from DNA polymer restricts its ability for more precise measurements, such as accurately determining the concentration of DNA nanoparticles in solution through NTA counting. In **Figure 3A**, scattering NTA detected ~ $7.1\times10^5 \pm 4.7\times10^5$ particles/ml for rectangular DNA origami, despite DNA origami was prepared at ~ 6.0×10^8 particles/ml (1 pM) as quantified by UV absorbance at 260 nm. The raw scattering intensity for detected DNA origamis ranged from 1 – 20 a.u., while more DNA origamis were scattered too weak to be detected. The low scattering intensity of DNA origami resulted in a poor NTA particles counting showing a concentration three orders of magnitude lower than the actual concentration determined by UV absorbance. Solid gold nanoparticles (GNPs), on the other hand, exhibited strong scattering signals in solution. In **Figure 3B**, the scattering NTA measurement of 50 nm GNPs showed a total particle concentration of ~ $5.9\times10^8 \pm 0.6\times10^8$ particles/ml, which closely matched the prepared

nanoparticles concentration of ~ 6.0×10^8 particles/ml. The raw scattering intensity of the nanoparticles ranged from 200 to 1200 a.u., making them well-suited for NTA counting.

To increase the detection sensitivity, we next used fluorescent NTA to analyze DNA origami nanostructures. To make DNA nanostructures fluorescent, we chose to label DNA origami with intercalation dyes. Intercalation dyes generally refer to a group of molecules that can insert into planar bases pairing of dsDNA (**Figure 4A**). The inserted dyes will exhibit much stronger fluorescence than uninserted dye molecules, which is widely used for analyzing dsDNA molecules.[37] In **Figure 4B**, the fluorescence emission of a DiYO™-1 (Diyo) was largely enhanced by binding to a DNA origami as compared to free Diyo. In **Figure 4C**, by titrating the incubation ratio of Diyo-to-DNA origami, the maximal fluorescence emission was obtained when Diyo was added into DNA origami with a molar ratio of 800:1. The higher Diyo-to-DNA origami ratio than 800 resulted in a decreased fluorescence signal. In **Figure 4D**, Diyo-intercalated, rectangular DNA origami was detected by fluorescent NTA, showing two peaks at ~ 72 nm for monomer and ~ 102 nm for dimer. The increased particles population at ~ 102 nm suggested a potential DNA origami aggregation induced by Diyo intercalation. The total DNA particles concentration was ~ 3.2×10^7 ± 1.6×10^7 particles/ml, which was much higher than that given by scattering NTA (~ 7.1×10^5 particles/ml). However, this concentration measured by fluorescent NTA was still significantly lower than the prepared concentration at ~ 6.0×10^8 particles/ml. To further enhance the fluorescent signals of DNA origami, we incubated DNA nanostructures with anoter intercalation dye of QuantiFluor® (QF), which was used for quantifying dsDNA. As shown in **Figure 4E**, we titrated the incubation ratio of QF to DNA origami for particles counting on NTA. By increasing the QF-to-DNA origami ratios from 42 to 169, the measured concentrations of DNA nanoparticles by NTA were increased from ~ 3.1×10^7 ± 3.2×10^6 particles/ml to ~ 4.1×10^8 ± 1.3×10^7 particles/ml. Using

the optimized ratio of 169, fluorescent NTA was used to characterize QF-intercalated DNA origami with the primary peak size at ~ 63 nm and a minor peak at ~ 95 nm. The total concentration of DNA nanoparticles was $5.4\times10^8 \pm 0.7\times10^8$ particles/ml, which was consistent with the prepared DNA origami concentration at ~ 6.0×10^8 particles/ml. Based on the above results, QF-intercalated DNA origami was more sensitive than Diyo-intercalated DNA origami for fluorescent NTA measurement. This offers an alternative method to determine DNA origami concentration in solution, aside from UV absorbance. Furthermore, QF intercalation induced less aggregation of DNA origami than Diyo intercalation.

4. Conclusion

In summary, we investigate the use of DLS and NTA to analyze DNA origami nanostructures for their sizes distribution and particles concentrations. Compared to DLS, NTA demonstrated higher resolution of size measurement with smaller FWHM, especially for characterizing the size and population distribution of multiple components. To increase the sensitivity of NTA measurement, we used intercalation dyes to enhance the fluorescence signals of DNA origami. Through optimizing intercalation dyes and the dye-to-DNA origami ratio, fluorescent NTA successfully quantified the total concentration of QF-intercalated DNA nanostructures, aligning closely with values obtained by UV absorbance at 260 nm. This optimized fluorescent NTA method offers an alternative approach for determining the concentration of DNA nanostructures in addition to commonly used UV absorbance quantification. Overall, the scattering and fluorescent NTA provides a robust and sensitive method to precisely characterize DNA origami nanostructures for their size distribution, multimerization and particle concentrations in

solution. This detailed information will be useful for quality control, material preparation and various application of DNA nanotechnology.

Origami	DLS (Number)				NTA					
	Peak 1		Peak 2		Peak 1		Peak 2		Peak 3	
	Peak center (nm)	FMWH (nm)	Peak center (nm)	FMWH (nm)	Peak center (nm)	FMWH (nm)	Peak center (nm)	FMWH (nm)	Peak center (nm)	FMWH (nm)
Rectangular	78.2 ± 0.8	27.6 ± 2.6	104.1 ± 7.3	48.2 ± 9.2	54.8 ± 0.1	11.1 ± 0.1	92.1 ± 0.9	21.2 ± 0.3	-	-
Triangular	A broad peak with the maximal peak height ~80 nm				65.8 ± 0.2	18.7 ± 0.5	124.9 ± 0.5	23.7 ± 1.1	195.8 ± 2.1	17.7 ± 5.2

Table 1. Size distribution and resolution of DNA origami as characterized by DLS and NTA.

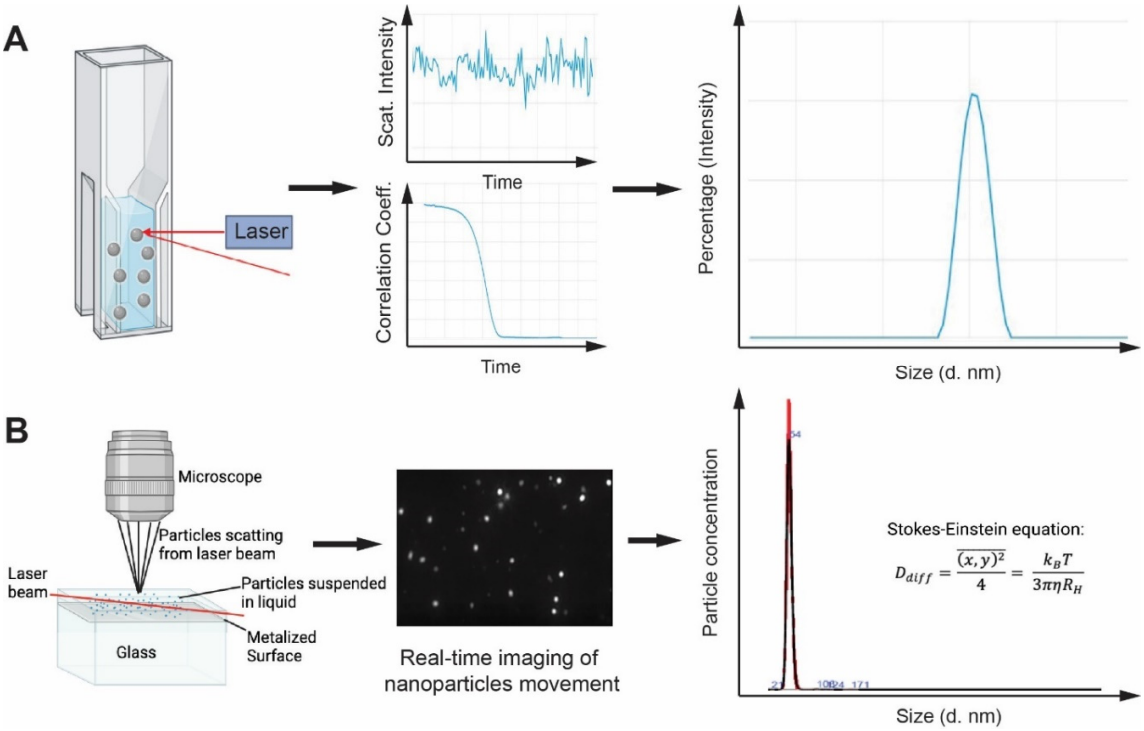

Figure 1 Basic principles of DLS and NTA. (**A)** A hypothetical scenario for light scattering of nanoparticles and how particle sizes are determined by the correlation function of the scattered light intensity. **(B)** Schematic of the optical configuration used in NTA and the real-time capture of particles movement by scattering or fluorescence. The size and concentration of nanoparticles that are individually tracked are analyzed by NTA software based on the Stokes-Einstein equation.

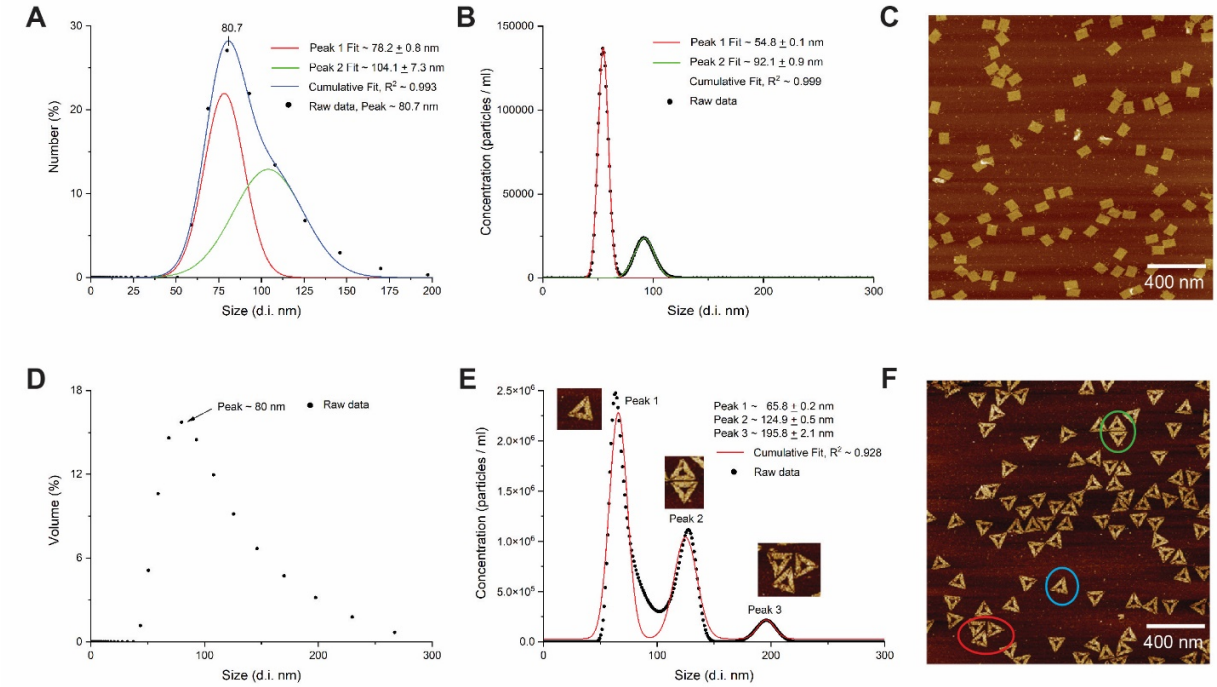

Figure 2. DLS and NTA for characterizing DNA origami structures by scattering signals. (A) DLS analysis of rectangular DNA origami at a concentration of ~ 7 nM showed a broad peak (depicted by black dots) spanning from ~ 50 to 150 nm, with potential distinct peaks at ~ 78 nm and 104 nm as indicated by peak fitting. **(B)** NTA scattering analysis of the same rectangular DNA origami at ~ 1 pM clearly showed two distinct peaks at ~ 55 nm (major monomer) and 92 nm (minor dimer). **(C)** Rectangular DNA origami structure was imaged by AFM on a 2D mica surface. **(D)** DLS characterization of triangular DNA origami at a concentration of ~ 7 nM exhibited a broad peak ranging from ~ 50 to 250 nm, suggesting the multimerization of DNA origamis. **(E)** Scattering NTA analysis of the same triangular DNA origami at 1 pM revealed three distinct peaks at ~ 66 nm (monomer), 125 nm (dimer), and 196 nm (trimer). **(F)** AFM imaging showed the formation of monomers (blue circle), dimers (green circle), and trimers (red circle) of triangular DNA origami.

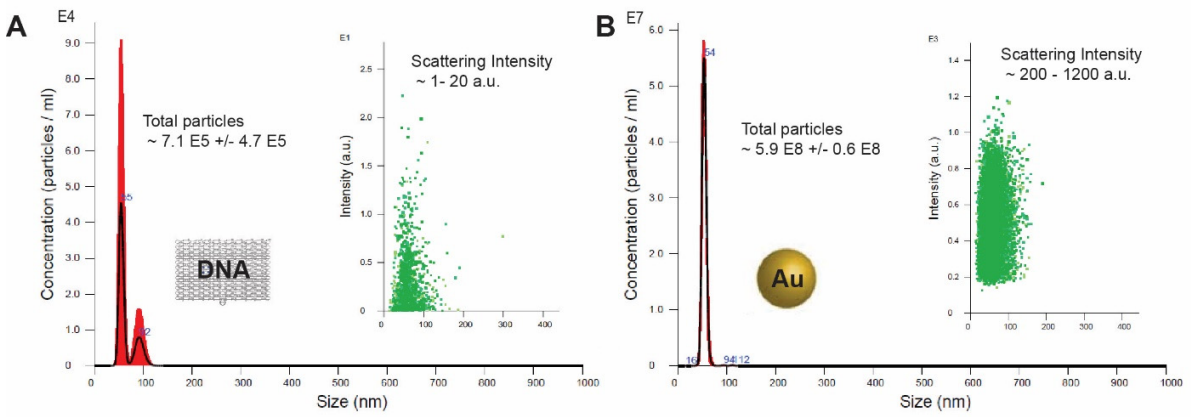

Figure 3. Scattering NTA for characterizing DNA origami and GNPs. (A) Scattering NTA detected ~ $7.1\times10^5 \pm 4.7\times10^5$ particles/ml for DNA origami, despite the preparation of DNA origami at ~ 6.0×10^8 particles/ml (1 pM). The raw scattering intensity for DNA origamis ranged from 1 – 20 a.u. **(B)** Scattering NTA detected 50 nm GNPs at ~ $5.9\times10^8 \pm 6.1\times10^7$ particles/ml, with a mean size ~ 53.8 ± 0.2 nm. The prepared GNPs were at ~ 6.0×10^8 particles/ml. The raw scattering intensity for GNPs ranged from 200 – 1200 a.u.

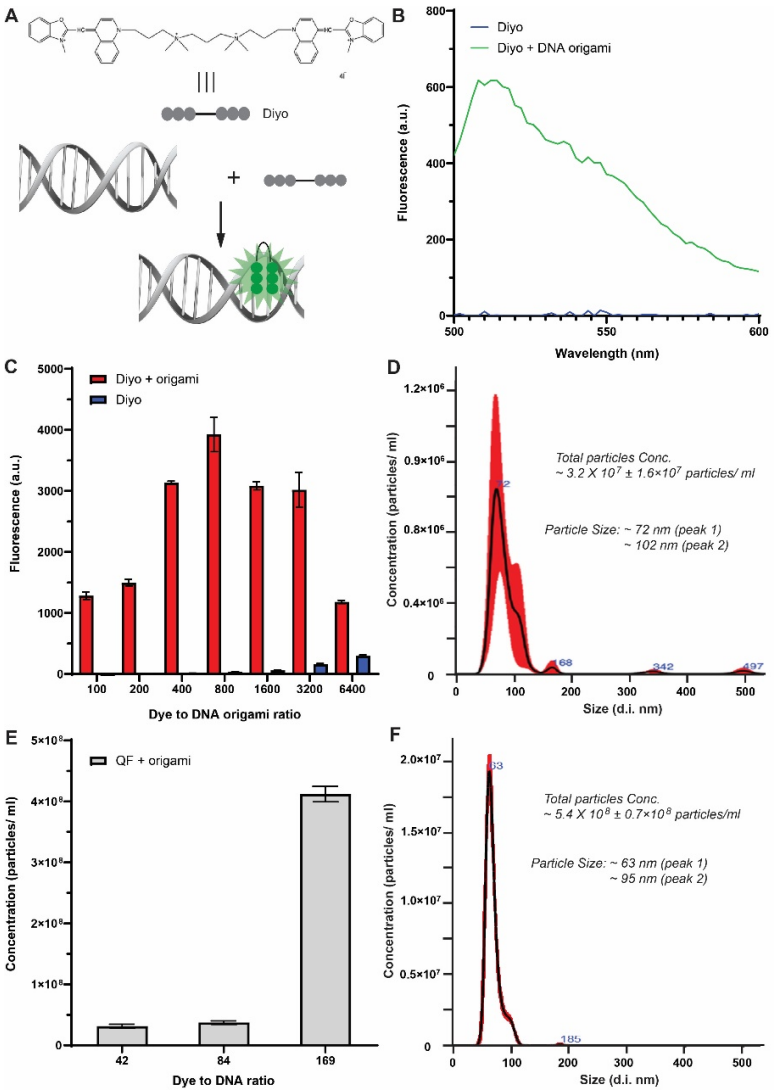

Figure 4. Fluorescent NTA for characterizing the size and concentration of DNA origami. (A) Dye molecules (Diyo) are intercalated into double-stranded DNA to enhance fluorescence. **(B)** Enhanced fluorescence emission by intercalating diyo into a rectangular DNA origami. **(C)** Titration of the Diyo-to-DNA origami ratio for optimizing fluorescence signals. **(D)** Fluorescent NTA of Diyo-intercalated rectangular DNA origami at a ratio of 800:1. **(E)** Titration of QF-to-DNA origami ratio for optimizing fluorescent NTA counting of DNA nanoparticles. **(F)** Fluorescent NTA of QF-intercalated rectangular DNA origami at a ratio of 169:1. For all measurements, DNA origami was prepared at ~ 6×10^8 particles/ml (~ 1 pM). Error bar, standard deviation of at least three measurements.

ASSOCIATED CONTENT

AUTHOR INFORMATION

Corresponding Authors

*E-mail: Jinglin Fu, jf604@camden.rutgers.edu

Author Contributions

Q.Z. and J.F. designed experiments, Q.Z., A.E. and A.S. ran experiments and collected data. The manuscript was drafted and revised by Q.Z. and J.F. All authors have given approval to the final version of the manuscript.

Notes

The authors declare no competing financial interest.

Supporting Information Available

Size distribution based on three modes of number, volume, and signal intensity tested by DLS (Figure S1); DNA origami maps (Figure S2-S3); thermal annealing program for preparing DNA nanostructures (Table S1), DNA sequences (Table S2-S3).

ACKNOWLEDGMENT

This work was supported by a PECASE award to J.F. (W911NF1910240), a DoD DURIP (W911NF2010107), a NSF MRI (2215917) and a NSF PFI award (2141141). J.F. also appreciates the support from Busch Biomedical Grant. Q.Z. and A.E. appreciate the support from Rutgers-Camden Chancellor's Grant for Independent Student Research. A.S. appreciates the support of the Arts and Sciences OMIC Summer Research Grant and Undergraduate Apprenticeship from AEOP.

Authors are also grateful to the advice and help from Jia Nong and Zhicheng Wang for NTA measurement.

Reference

1. Y. Krishnan, N. C. Seeman, *Chem. Rev.*, **2019**, 119, 6271-6272.

2. M. Bathe, P. W. K. Rothemund, *MRS Bull.*, **2017**, 42, 882-888.

3. J. Fu, M. Liu, Y. Liu, H. Yan, *Acc. of Chem. Res.*, **2012**, 45, 1215-1226.

4. P. Zhan, A. Peil, Q. Jiang, D. Wang, S. Mousavi, Q. Xiong, Q. Shen, Y. Shang, B. Ding, C. Lin, Y. Ke, N. Liu, *Chem. Rev.*, **2023**, 123, 3976-4050.

5. J. Fu, M. Liu, Y. Liu, N. W. Woodbury, H. Yan, *J. Am. Chem. Soc.*, **2012**, 134, 5516-5519.

6. J. Fu, Z. Wang, X. H. Liang, S. W. Oh, E. St Iago-McRae, T. Zhang, *Top. Curr. Chem.*, **2020**, 378, 38-38.

7. Z. Zhao, J. Fu, S. Dhakal, A. Johnson-Buck, M. Liu, T. Zhang, N. W. Woodbury, Y. Liu, N. G. Walter, H. Yan, *Nat. Commun.*, **2016**, 7, 10619.

8. Y. Choi, B. K. Cho, S. H. Seok, C. Kim, J. H. Ryu, I. C. Kwon, *J. Controlled Release*, **2023**, 360, 672-686.

9. J. Fu, S. W. Oh, K. Monckton, G. Arbuckle-Keil, Y. Ke, T. Zhang, *Small*, **2019**, 15, 1900256.

10. J. Fu, Y. R. Yang, A. Johnson-Buck, M. Liu, Y. Liu, N. G. Walter, N. W. Woodbury, H. Yan, *Nat. Nanotechnol.*, **2014**, 9, 531-536.

11. N. Liu, T. Liedl, *Chem. Rev*, **2018**, 118, 3032-3053.

12. Z. Yang, H. Liu, D. Liu, *NPG Asia Mater.*, **2015**, 7, e161-e161.

13. S. W. Oh, A. Pereira, T. Zhang, T. Li, A. Lane, J. Fu, *Angew. Chem. Int. Ed.*, **2018**, 57, 13086-13090.

14. T. Zhang, J. Nong, N. Alzahrani, Z. Wang, S. W. Oh, T. Meier, D. G. Yang, Y. Ke, Y. Zhong, J. Fu, *ACS Appl. Mater. Interfaces*, **2019**, 11, 29512-29521.

15. Q. Jiang, Y. Shang, Y. Xie, B. Ding, *Adv. Mater.*, **2023**, 2301035.

16. X. Wu, C. Yang, H. Wang, X. Lu, Y. Shang, Q. Liu, J. Fan, J. Liu, B. Ding, *J. Am. Chem. Soc.*, **2023**, 145, 9343-9353.

17. R. Veneziano, T. J. Moyer, M. B. Stone, E.-C. Wamhoff, B. J. Read, S. Mukherjee, T. R. Shepherd, J. Das, W. R. Schief, D. J. Irvine, M. Bathe, *Nat. Nanotechnol.*, **2020**, 15, 716-723.

18. E. A. Hemmig, C. Creatore, B. Wünsch, L. Hecker, P. Mair, M. A. Parker, S. Emmott, P. Tinnefeld, U. F. Keyser, A. W. Chin, *Nano Lett.*, **2016**, 16, 2369-2374.

19. X. Zhou, S. Mandal, S. Jiang, S. Lin, J. Yang, Y. Liu, D. G. Whitten, N. W. Woodbury, H. Yan, *J. Am. Chem. Soc.*, **2019**, 141, 8473-8481.

20. É. Boulais, N. P. D. Sawaya, R. Veneziano, A. Andreoni, J. L. Banal, T. Kondo, S. Mandal, S. Lin, G. S. Schlau-Cohen, N. W. Woodbury, H. Yan, A. Aspuru-Guzik, M. Bathe, *Nat. Mater.*, **2018**, 17, 159-166.

21. M. A. B. Baker, A. J. Tuckwell, J. F. Berengut, J. Bath, F. Benn, A. P. Duff, A. E. Whitten, K. E. Dunn, R. M. Hynson, A. J. Turberfield, L. K. Lee, *ACS Nano*, **2018**, 12, 5791-5799.

22. R. Li, H. Chen, H. Lee, J. H. Choi, *Appl. Sci.*, **2021**, 11, 2357.

23. L. Mallik, S. Dhakal, J. Nichols, J. Mahoney, A. M. Dosey, S. Jiang, R. K. Sunahara, G. Skiniotis, N. G. Walter, *ACS Nano*, **2015**, 9, 7133-7141.

24. J. Stetefeld, S. A. McKenna, T. R. Patel, *Biophys. Rev.*, **2016**, 8, 409-427.

25. B. Lorber, F. Fischer, M. Bailly, H. Roy, D. Kern, *Biochem. Mol. Biol. Educ.*, **2012**, 40, 372-382.

26. W. T. Winter, *J. Polym. Sci.*, **1983**, 21, 1020-1020.

27. O. Annunziata, D. Buzatu, J. G. Albright, *Langmuir*, **2005**, 21, 12085-12089.

28. J. D. Fiedler, S. D. Brown, J. L. Lau, M. G. Finn, *Angew. Chem. Int. Ed.*, **2010**, 49, 9648-9651.

29. M. Wright in *Nanoparticles in Biology, Medicine: Methods, Protocols*, (Ed. M. Soloviev) Humana Press, New York, **2012**, pp. 511-524.

30. B. Carr, M. Wright, *Innovations Pharm. Technol.*, **2008**, 26, 38-40.

31. J. Fu, Y. R. Yang, S. Dhakal, Z. Zhao, M. Liu, T. Zhang, N. G. Walter, H. Yan, *Nat. Protoc.*, **2016**, 11, 2243-2273.

32. S. W. Oh, Z. Wang, J. Fu, *Methods Mol. Biol.*, **2022**, 2487, 93-112.

33. Q. Zhang, Q. Jiang, N. Li, L. Dai, Q. Liu, L. Song, J. Wang, Y. Li, J. Tian, B. Ding, Y. Du, *ACS Nano*, **2014**, 8, 6633-6643.

34. Z. Wang, E. St. Iago-Mcrae, A. Ebrahimimojarad, S. Won Oh, J. Fu, *Langmuir*, **2022**, 38, 12594-12601.

35. J. Fu, K. Nguyen, *ACS Appl. Bio Mater.*, **2022**, 5, 1839-1845.

36. Q. Jiang, C. Song, J. Nangreave, X. Liu, L. Lin, D. Qiu, Z.-G. Wang, G. Zou, X. Liang, H. Yan, B. Ding, *J. Am. Chem. Soc.*, **2012**, 134, 13396-13403.

37. H. Ihmels, K. Faulhaber, D. Vedaldi, F. Dall'Acqua, G. Viola, *Photochem. Photobiol.*, **2005**, 81, 1107-1115.

Table of Contents Figure